

## 2 Experimental and calculation methods

...

Density functional theory (DFT) calculations were carried out with the Vienna ab initio simulation package (VASP) [64] using the Perdew-Burke-Ernzerhof (PBE) exchange correlation functional [65,66] and the PAW method [67,68].

To establish trends in total energy and net magnetic moment without using supercells, calculations were carried out using the virtual crystal approximation (VCA) with special PAW data sets. These data sets were constructed inspired by the *GW*-style data sets for Mn and Fe with frozen [Ne] core from the VASP distribution. They interpolate, using fractional charges, between Mn ( $Z = 15$  effective core charge) and Fe ( $Z = 16$  effective core charge). These were generated for  $Z = 15, 15.11, 15.17, 15.23, 15.33, 15.67, 16$  keeping these potentials as similar as possible. For Sn the standard potential with frozen [Kr] core was used.

VCA calculations were done in a primitive hexagonal cell with 8 atoms that was fully optimized ( $c$ ,  $a$ , internal coordinates) observing only symmetry requirements. The kinetic energy cutoff was 600 eV and a  $\Gamma$ -centred  $7 \times 7 \times 10$  **k**-point mesh with Methfessel-Paxton smearing of 1th order ( $\sigma = 0.1$  eV) was employed [70]. Spin-orbit coupling was used with two-component spinors [Hobbs, Steiner].

To obtain more relativistic models, some calculations were carried without the VCA. For these we used the same potentials with  $Z = 15$  (Mn) and  $Z = 16$  (Fe). A few checks were carried out repeating some calculations with potentials the standard VASP 54 distribution. We used the same cutoff and smearing as for VCA. Fixed hexagonal lattice parameters of  $a = 5.57$  Å and  $c = 4.45$  Å (cf. Table 1) were used. Fe and Mn were positioned randomly at the  $8h$  sites in a  $2 \times 2 \times 1$  super cell ( $a = 11.13$ ,  $c = 4.45$ ). Internal coordinates were optimised using both  $2 \times 2 \times 4$  and, in the final optimization steps for the “canted” magnetic structure,  $4 \times 4 \times 10$  **k**-points. The DOS were calculated with the  $4 \times 4 \times 10$  **k**-point mesh using the tetrahedron method [69].

### 3.4 Electronic and magnetic properties of $\text{Mn}_2\text{FeSn}$

The most striking finding of our study is the coexistence of FM and AFM spin structures below  $T_S$  around the composition  $\text{Mn}_2\text{FeSn}$ . Such out-of-plane canted spin structures were observed by Tagami *et al.* in a DFT study on  $\text{Mn}_{3-x}\text{Fe}_x\text{Sn}$  using the virtual crystal approximation (VCA) around the composition  $x = 0.5$ . We have also carried out DFT VCA calculations, considering several magnetic orderings: (i) FM  $\Gamma_2$  alignment with moments along  $c$ , (ii) FM in the  $ab$ -plane with moments according  $\Gamma_{10}$ , (iii)  $ab$ -plane AFM with  $\Gamma_8$  ordering, and (iv) the specific canted structure, combining  $\Gamma_2$  and  $\Gamma_8$  patterns, that ND reveals for  $x = 0.8$  and  $1.0$  (Fig. 5(a,b)). In the VCA Mn and Fe are replaced with the single magnetic species with a fractional core charge determined by  $x$ . The results are summarized in Fig. S5 (supplementary information). We find that  $c$ -axis FM is most stable for  $x \gtrsim 0.6$ . Indeed, as expected, in the Mn-rich limit ( $x \lesssim 0.4$ ) that  $ab$ -plane AFM ordering is more stable than  $c$ -axis FM. Moreover, the  $c$ -axis FM ( $ab$ -plane AFM) moment increases (decreases) with  $x$ , consistent with the experimental trend. In the crossover region at  $x = 0.5$  both the canted and the  $ab$ -plane FM are more stable, where the latter appears to be consistently slightly more stable than the former. This confirms the trend observed by Tagami *et al.* [cite Tagami] The trend is also similar to the ND results, however, where ND has canted moments at  $x = 1.0$  in the VCA the canted structure is unstable at this composition. Moreover,  $ab$ -plane FM ordering is slightly more stable than the canted structure, whereas ND shows canted to be preferred at 5 K. The VCA captures the trends, but results are not in quantitative agreement.

To go beyond VCA we use a supercell with eight formula units with Fe and Mn randomly distributed on the  $6h$  sublattice. Two magnetic structures were considered: (a) “FM”, with all moments initialized along  $c$ , i.e., like “ $T_2$ ” (b) “canted”, with all moments initialized with the canted ND pattern (Fig. 5(a,b)). Details on the moments are summarized in Table 4. The local densities of states are in Fig. 10.

After optimizing the moments, the FM has retained its collinear ordering along  $c$ . However, the size of the average Mn moment is relatively small ( $2.39 \mu_B$ ) and varies strongly from Mn to Mn with an r.m.s. deviation of  $0.6 \mu_B$ . Indeed the local Mn DOS’ are rather dissimilar (Fig. 10(a)).

The canted structure has much lower total energy than  $c$ -axis FM: 0.12 eV/f.u. In the “canted” structure the moments remain canted, but their orientations exhibit a large degree of disorder, see, Fig. 11. The Mn moments are on average larger ( $2.79 \mu_B$ ) and the variation in size has almost disappeared. The local DOS’ are also much more similar and The hybridisation in the local “minority” channels is strongly reduce, see Fig. 10(d-e). Moreover, a clear minimum at the Fermi level has developed. The Mn moments pull towards the  $ab$ -plane ( $\langle \theta_{\text{Mn}} \rangle = 25^\circ$ ) whereas the Fe moments are much closer to  $c$  ( $\langle \theta_{\text{Mn}} \rangle = 67^\circ$ ), i.e., they appear to favour the ordering of their “parent compounds” ( $x = 0$  and  $x = 3$ ).

The ND does not resolve the individual magnetic species, i.e., does not discriminate between Mn and Fe. The average FM ( $c$ -axis) moment of  $1.38 \mu_B$  can be directly compared and appears to agree well with the ND FM moment of  $1.40 \mu_B$ . To enable a rough comparison with the AF component, we symmetrise the moments with a simple averaging (rotating moments by either  $120^\circ$  or  $240^\circ$  and building the vector sum). The resulting AFM component

moment is  $1.97 \mu_B$ , to be compared to the ND value of  $2.37 \mu_B$ . Given the very small size of the supercell, with only 16 Mn and 8 Fe, averaging might be imperfect. The underestimation could also point to slightly more local order in the material, e.g., by a small tendency for like species to cluster. The Fe local moment ( $2.10 \mu_B$ ) is comparable to the moment estimated from the hyperfine field using the proportionality factor ( $1.98 \mu_B$ ).

### Reviewer #3 for manuscript BW14449

*The paper provides an overview of the structural, magnetic and caloric properties of hexagonal (MnFe)3Sn, which is discussed as potential material for magnetocaloric applications. The authors combine a multitude of complementary advanced methodology like X-ray diffraction and spectroscopy, electron microscopy and neutron diffraction. Magnetic properties were analyzed using SQUID, VSM, and from theoretical side DFT. With this, the authors can paint a comprehensive picture of the material and identify a gradual transition in a comparatively narrow composition region from a non-collinear AFM to a collinear FM via a canted magnetic structure. In total, I consider this work of high quality and relevance for the readership of PRB and nearly ready for publication. The DFT part lacks a bit of the depth of the experimental investigation and raises a few technical questions, which should be clarified before publication.*

We thank the reviewer for the positive comments and valuable remarks. Below the comments of the reviewer are discussed point by point.

1. *“The calculations mainly report some magnetic moments and energy differences between competing phases which are in fair agreement with experiment but falls short to demonstrate its advertised role as “an effective tool to identify the potential of magnetocaloric materials”. In principle, a lot more could be done with DFT, from structural properties via orbital magnetism to Mössbauer parameters. The electronic DOS in Fig. 10 also does not really contribute to the understanding of the experimental findings. Right now, it is hardly discussed at all and could possibly move to the SM.”*

When investigating novel magnetocaloric materials, the number of magnetic sites within a unit cell and the predicted magnitude of the magnetic moments at each magnetic site are crucial for potential applications. Additionally, the nature of the magnetic ordering plays an essential role, as a ferromagnetic (FM) to paramagnetic (PM) transition is generally preferred. In this context, our DFT calculations have made a valuable contribution to this study. Regarding the electronic density of states (DOS) shown in Fig. 10 (Section 3.4), the discussion focuses on the primary contributions of the 3d electrons from Mn and Fe and their corresponding magnetic moments. As this figure is central to understanding the electronic and magnetic properties of the system, we prefer to retain it in the main text.

We have reworked the DFT part, and carried out additional calculations. Indeed Fig. 10, on a collinear FM structure with an ordered atomic structure, was not very relevant to our material at the  $Mn_2FeSn$  composition. We have replaced it with the DOS for a small supercell (8 f.u., no VCA) with random Fe/Mn positioned on the transition metal sublattice. The new figure 10 contrast the FM collinear order and the canted non-collinear magnetic structure (that we consider the best approximation to the “real world” system). Extensive details on the results of these two calculations are given in a revised Table 4. The discussion in section 3.4 has been modified accordingly. A figure 11 with snapshots of the canted magnetic structure of the disordered model has been added.

Orbital moments are quite small, and we prefer not to discuss them. The Mössbauer measurements clearly demonstrate the rotation of the Fe moment from out-of-plane to in-plane with increasing temperature. The derived local moment is in reasonable agreement with our canted DFT model. We don’t expect to learn much from more extensive calculations where achieving k-point converge is probably very tedious. The orientation of the field gradient tensor is already apparent from the crystal structure.

2. *“The most important question relates to the magnetic structure of the AFM. It does not become clear to me, whether the authors considered a non-collinear arrangement as identified in the experiment and/or spin-orbit coupling, possibly with spin canting. It should be stated clearly in how far these experimental findings were considered or neglected for whatever reason. Furthermore, the calculations address both, stoichiometric  $Mn_2FeSn$  (I assume in an ordered cell) and disordered configurations in the framework of the VCA. The calculated structures of should be identifiable in both cases (space group, Wyckoff positions...). Were the same lattice parameters were used in the VCA case, or was optimization involved? This should be stated clearly as well. Personally, I would expect considerable changes over the entire composition range. The stoichiometric case and the VCA calculations use a quite different technical setup, in particular the plane wave cutoff energy is more than twice as large in the latter case. Is there a special reason for this? The VCA is used rarely for these materials, as it is generally considered (right or wrong) as not very accurate. It would thus be of help for future reasearch, if the authors compared their VCA results directly to the stoichiometric case (e.g. through the DOS, total energies and magnetic moments in Table 4 and/or the corresponding Figures in the SM) to give a better understanding of benefits and limitations this rather basic model of alloying.”*

TABLE I. **Table 4** Details of the local magnetic moments for the supercell calculations. The average sizes ( $\langle m_{\text{Mn}} \rangle$  and  $\langle m_{\text{Fe}} \rangle$ ), the r.m.s. deviations from the averages (in parentheses) and the average angles of the moments with the *ab*-plane ( $\langle \theta_{\text{Mn}} \rangle$  and  $\langle \theta_{\text{Fe}} \rangle$ ). Symmetrized local moments: size ( $m$ ), *ab*-plane component (AFM) and *c*-axis component (FM).

|                   | Mn                              |                      |                                      | Fe                              |                      |                                      | symmetrized moments ( $\mu_{\text{B}}$ ) |                 |                |
|-------------------|---------------------------------|----------------------|--------------------------------------|---------------------------------|----------------------|--------------------------------------|--|-----------------|----------------|
|                   | $\langle m_{\text{Mn}} \rangle$ | ( $\mu_{\text{B}}$ ) | $\langle \theta_{\text{Mn}} \rangle$ | $\langle m_{\text{Fe}} \rangle$ | ( $\mu_{\text{B}}$ ) | $\langle \theta_{\text{Fe}} \rangle$ | $m$                                      | $m(\text{AFM})$ | $m(\text{FM})$ |
| <i>c</i> -axis FM | 2.39                            | (0.58)               | 87.28°                               | 2.20                            | (0.15)               | 88.97°                               |  |                 |                |
| canted            | 2.79                            | (0.08)               | 25.01°                               | 2.11                            | (0.12)               | 67.06°                               | 1.979                                    | 1.418           | 1.380          |
| ND at 5 K         |                                 |                      |                                      |                                 |                      |                                      | 2.37                                     | 1.91            | 1.40           |

We need to discuss these comments and questions with Gilles. I think he will provide a suitable explanation.

Indeed, the most important is the AFM magnetic structure. We have considered non-collinear arrangements as identified in the experiment in both the VCA (with new results added) and in the supercell model mentioned above. With the VCA we can demonstrate a trend: there is a small composition range, between the *ab*-plane AFM (small  $x$ ) and collinear FM were a canted and a non-collinear with net moment ( $\Gamma_{10}$ , see Table S1) are more stable. These are exactly the configurations that follow from our neutron diffraction (below and above  $T_S$  respectively). Their order seems, however, wrong, and the stable VCA composition range is very different from our experiments. Without the VCA and with the supercell models, we see a clear stabilisation of a canted structure at the correct composition  $x = 1$ ,  $\text{Mn}_2\text{FeSn}$ . The VCA gives trends but is not quantitatively reliable.

All calculations have now been carried out with the same, high cutoff and the same kind of potentials. All were done with a non-collinear formalism including spin-orbit interaction. The description of technical details in section 2 has been modified accordingly. Figure S5 on the VCA in the SI has been modified and extended. It allows for an easy comparison with the recent (2024!) VCA study on the same system by Tagami et al. [Jpn. J. Appl. Phys. 63, 023001 (2024)]. They observe non-collinear structure, similar to ours, but, as far as we understand, did not consider the specific spin ordering patterns that we obtain from ND ( $\Gamma_2$  combined with  $\Gamma_8$  and  $\Gamma_{10}$ ).

[Hobbs] D. Hobbs, G. Kresse, J. Hafner, Phys. Rev. B **62**, 1156 (2000).

DOI: <https://doi.org/10.1103/PhysRevB.62.11556>

[Steiner] S. Steiner, S. Khmelevskiy, M. Marsmann, G. Kresse, Phys. Rev. B **93**, 224425 (2016).

DOI: <https://doi.org/10.1103/PhysRevB.93.224425>

[VESTA] K. Momma and F. Izumi, “VESTA 3 for three-dimensional visualization of crystal, volumetric and morphology data,” J. Appl. Crystallogr., 44, 1272-1276 (2011).

DOI: <https://doi.org/10.1107/S0021889811038970>

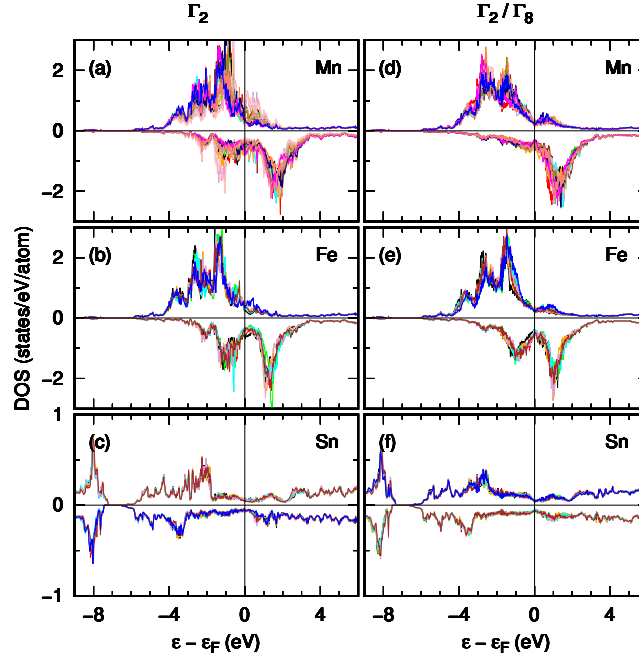


FIG. 1. **Figure 10** Local, site-projected DOS for the supercells with  $\text{Mn}_{16}\text{Fe}_8\text{Sn}_8$  and random Mn/Fe positions. (a-c) The  $c$ -axis FM magnetic structure, with  $\Gamma_2$ -like moment arrangements. (d-f) The canted magnetic structure, with a mix of  $\Gamma_2$  and  $\Gamma_8$  like moments. Of course the  $\Gamma$ -symmetry labels do not strictly apply, as the random placement of the TM on the  $6h$  sublattice breaks all symmetry. For the canted magnetic structure, the majority/minority DOSs (positive/negative) are shown relative to axes defined by the local magnetic moments (i.e. the energy-resolved local magnetization is projected onto the magnetization vector in the PAW sphere).

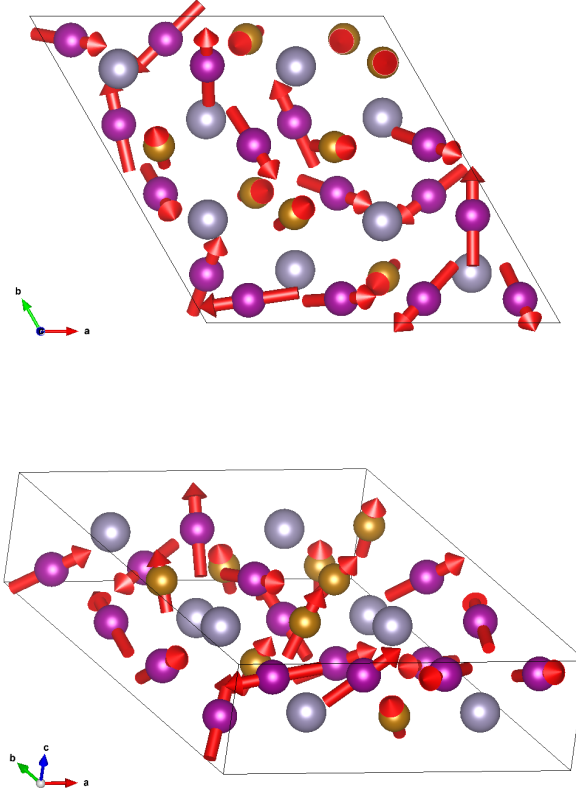


FIG. 2. **Figure 11** Magnetic moments in the  $\text{Mn}_{16}\text{Fe}_8\text{Sn}_8$  shown from several viewing angles. Picture made with VESTA. Mn purple, Fe gold, Sn grey spheres. [cite VESTA]

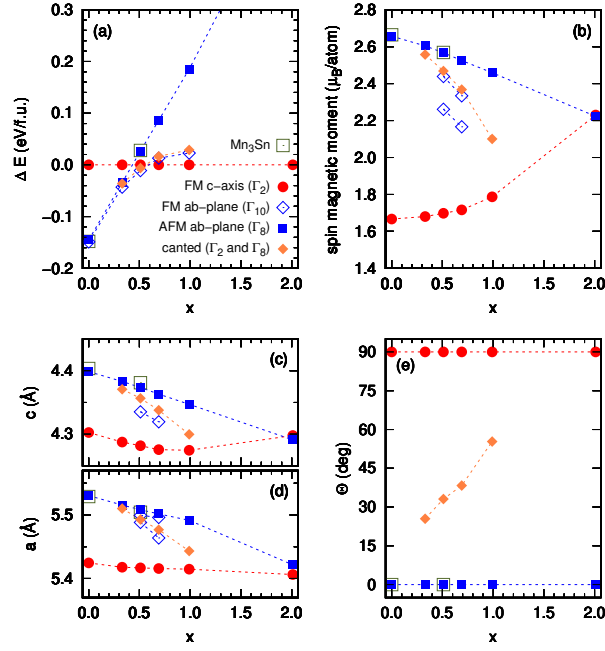


FIG. 3. **S5** VCA DFT results as a function of Fe content  $x$ : (a) Total energy per f.u.  $\text{Mn}_{3-x}\text{Fe}_x\text{Sn}$  relative to the total energy of the collinear FM magnetic structure with magnetic moment along the  $c$ -axis. (b) The size of the local magnetic moment. (c) The  $a$  and  $c$  lattice parameters. (d) The angle of the local moment with the  $ab$ -plane. Note that for  $\Gamma_{10}$  ordering the symmetry is broken, making that all three lattice vectors have different length and that there are two different magnetic moment sizes. The FM moment in the  $ab$ -plane is strongly dependent on  $x$ . For  $x = 0.51$  it is 4.1  $\mu_B/\text{f.u.}$  and for  $x = 0.99$  it is 5.4  $\mu_B/\text{f.u.}$